Chapter 8

Dielectric and Mechanical properties of Zr doped $CaCu_3Ti_4O_{12}$/ Poly(vinylidene fluoride) Composites

Structural, dielectric and mechanical properties of Zr doped CCTO / PVDF composites are discussed in this chapter. $CaCu_3Ti_4O_{12}$ (CCTO) and Zr doped $CaCu_3Ti_4O_{12}$ (CCTZO) have been prepared by solid state ceramic method. Zr doping in CCTO results in a considerable improvement in the dielectric properties of CCTO. CCTZO dispersed PVDF (PVDF-ZrC) composites have been prepared by melt extrusion method. CCTZO dispersion in PVDF improves the thermal, dielectric as well as mechanical properties of PVDF-ZrC composites.

8. Results and discussion

8.1. Structural Analysis

X-ray diffraction patterns of CCTZO, PVDF and composites containing 10, 20 and 50 wt % CCTZO in PVDF matrix are shown in Fig 8.1. In case of CCTZO, the diffraction peaks corresponding to reflections (220), (310), (222), (321), (400), (422) and (440) at 2θ values of 34.2°, 38.5°, 42.3°, 45.8°, 49.2°, 61.3° and 72.2° respectively confirms the formation of single phase compound [Sinclair et al (2002)]. No secondary phase is present in CCTZO. Pure PVDF crystallizes in α phase with characteristic 2θ peaks at 17.7°, 18.7°and 19.9°, corresponding to (100), (020) and (110) crystal planes respectively [Varma et al (2010)]. Intensity of three major peaks (220), (400) and (422) of CCTZO increases with increase in the content of CCTZO in the composites. Predominance of CCTZO phase is clearly visible in the PVDF-50ZrC composite in its XRD patterns as intensity of diffraction peaks of PVDF decreases as the content of CCTZO increases in the composites.

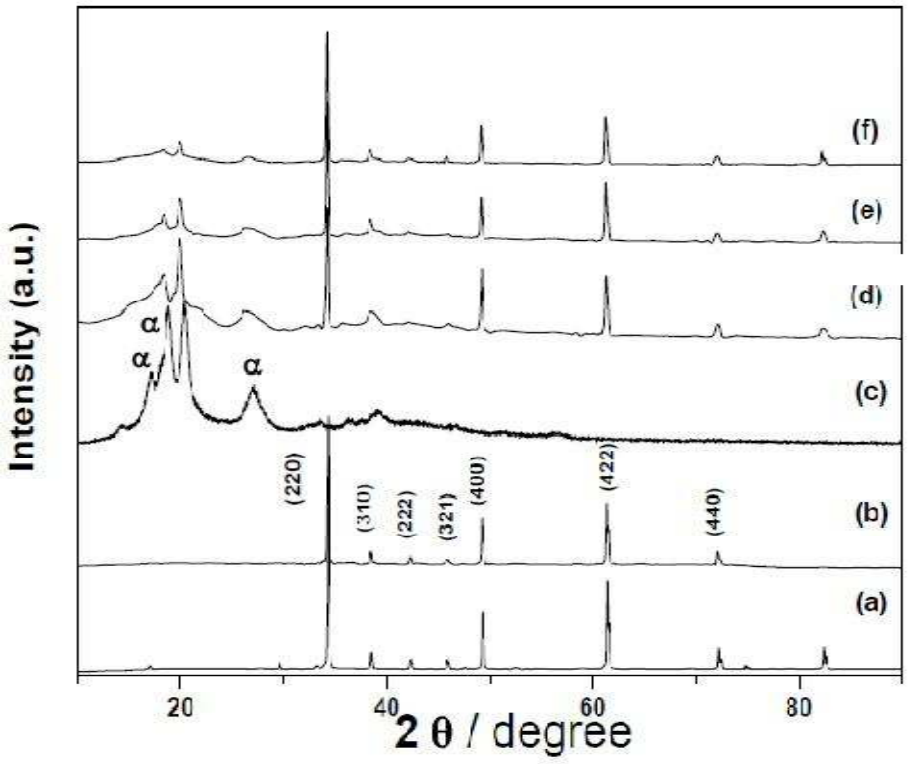

Figure 8.1 X-ray diffraction patterns for (a) CCTO, (b) CCTZO, (c) PVDF, (d) PVDF-10ZrC, (e) PVDF-20ZrC and (f) PVDF-50ZrC composites

8.2. Surface morphology

SEM micrographs of pure PVDF and PVDF-ZrC composites are shown in Fig 8.2. Spherulitic morphology of PVDF is drastically changed by the dispersion of CCTZO in it. At low filler concentration, CCTZO particles are well dispersed in the PVDF matrix while at higher filler concentration, the inter particle distance decreases leading to the formation of well connected dense network structure. This can be seen from SEM micrograph of the PVDF-50ZrC composite. These morphological changes influence the properties of the composites.

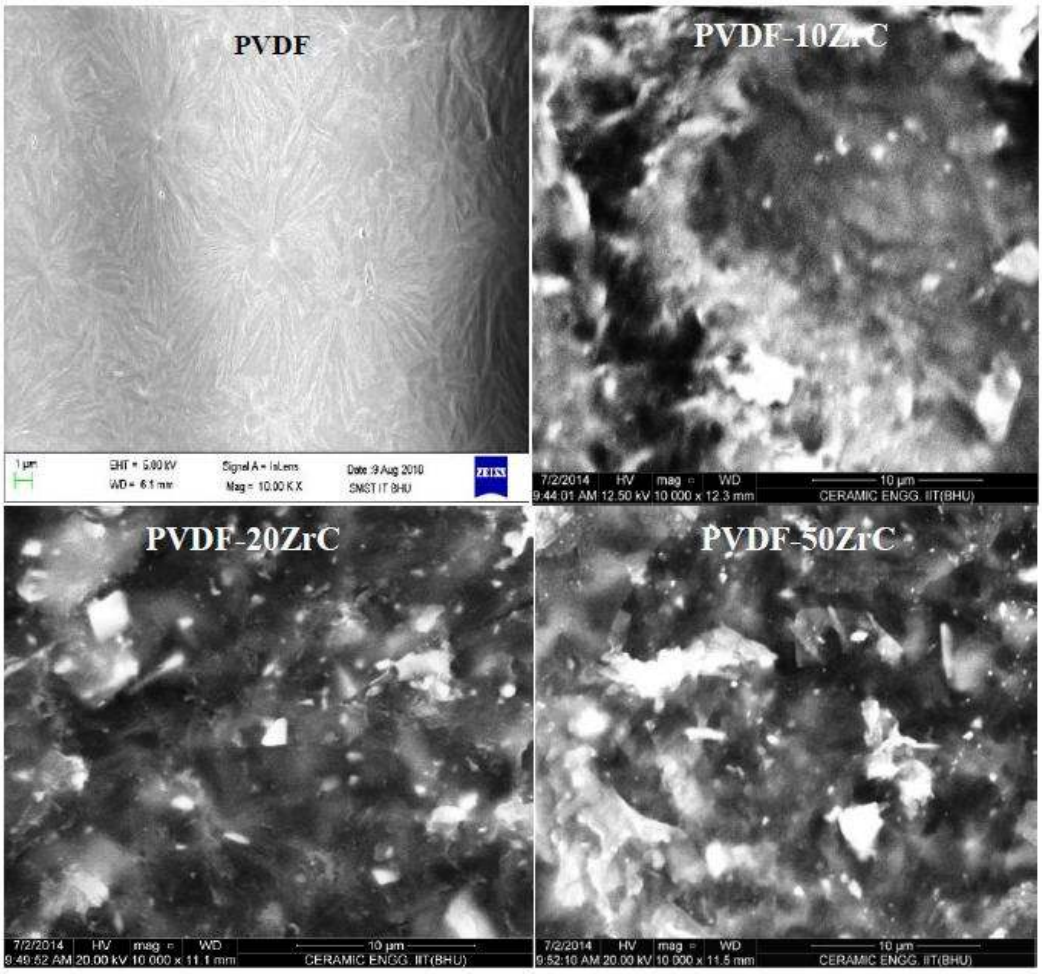

Figure 8.2 Scanning electron micrographs of PVDF, PVDF-10ZrC, PVDF-20ZrC and PVDF-50ZrC composites.

8.3. Thermal behavior

Thermogravimetric analysis (TGA) has been done to study the thermal stability of the polymer and the composites. Thermograms recorded for the pure PVDF and its composites are shown in Fig 8.3. It is observed that pure PVDF is stable up to 400°C and complete degradation of the polymer occurs at around 500°C. CCTZO filler shifts the degradation temperature to higher side i.e. from 442^0C in PVDF to 444^0C, 451^0C and 466^0C in PVDF-10ZrC, PVDF-20ZrC and PVDF-50ZrC respectively. It shows that

addition of CCTZO improves the thermal stability of the composites. This also indicates interaction between the polymer and ceramic particles.

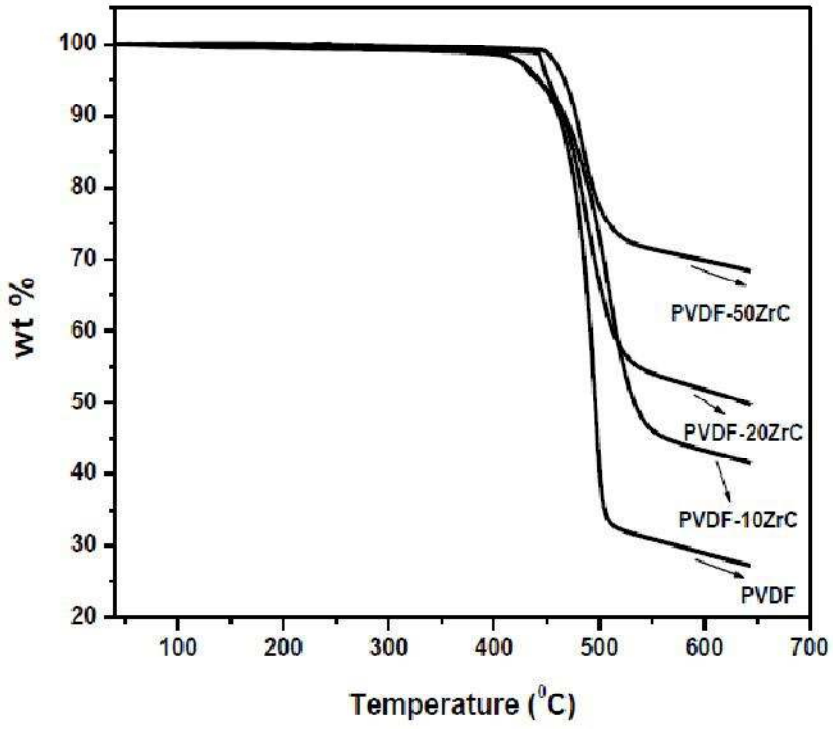

Figure 8.3 TGA of pure PVDF, PVDF-10ZrC, PVDF-20ZrC and PVDF-50ZrC composites.

8.4. Mechanical properties

Figure 8.4 shows the stress-strain curves of PVDF and its composites. Considerable increase was observed in the value of Young's modulus of the composites. For PVDF, PVDF-10ZrC, PVDF-20ZrC and PVDF-50ZrC, the values are 810, 934, 1094 and 1202 MPa respectively (Fig 8.4 b) showing continuous increase with increasing CCTZO content. This increase in Young's modulus with increase in weight percent of the filler can be attributed to interaction between the stiffer ceramic filler and flexible PVDF matrix making composites stiffer as compared to pure PVDF. Elongation at the breaking point decreases from 30% in PVDF to 20%, 18% and 16% in PVDF-10ZrC, PVDF-20ZrC and PVDF-50ZrC composites respectively (Fig 8.4 c). Decrease in the elongation is because of the ceramic particles which prevent the PVDF chains from packing with one another. This increase in the Young's modulus with increase in filler concentration

can be attributed to increase in the resistance to the free movement of polymeric chains by much harder ceramic particles.

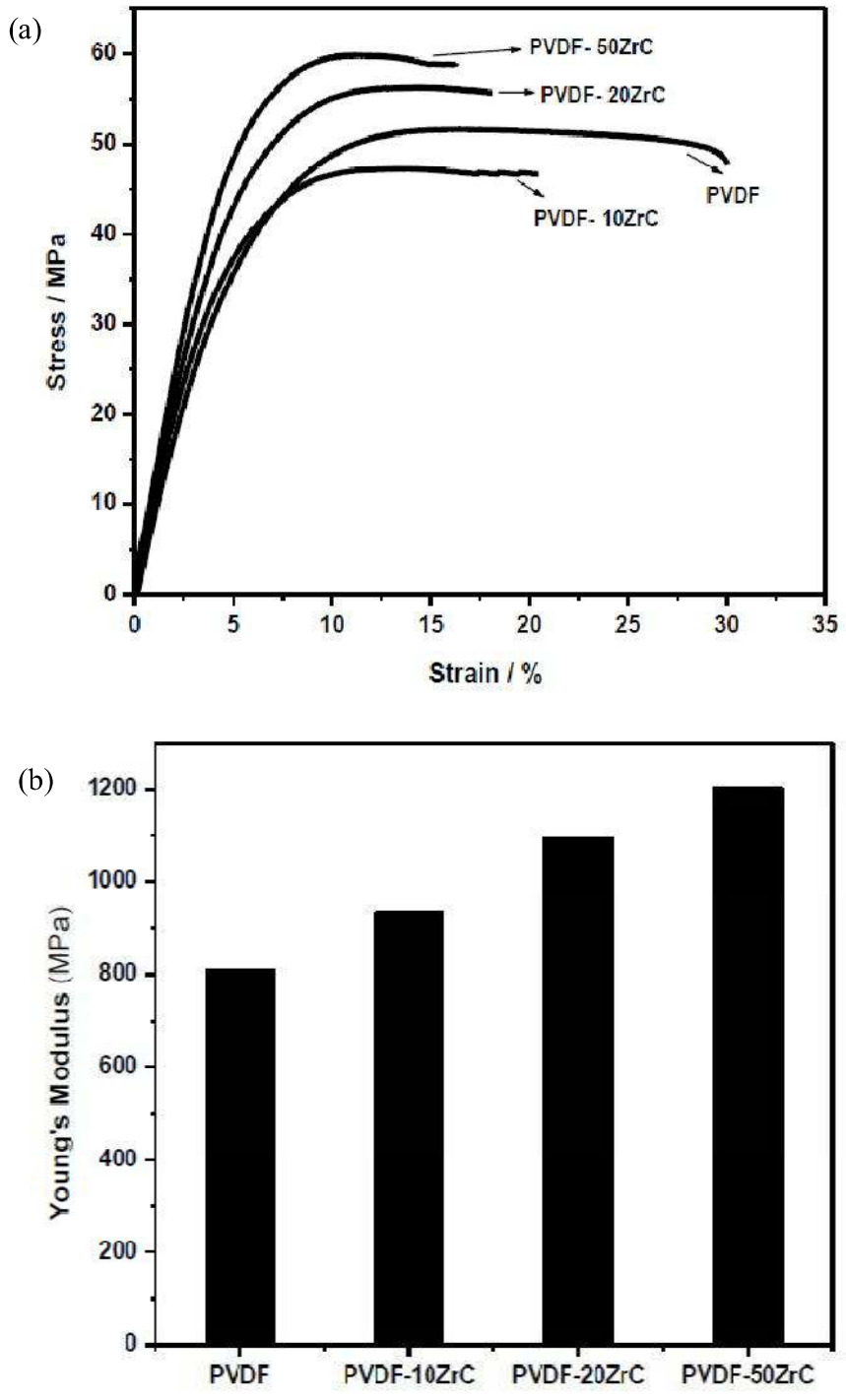

Figure 8.4 (a) Stress-strain curves for pure PVDF, PVDF-10ZrC, PVDF-20ZrC and PVDF-50ZrC composites, (b) Young's modulus of PVDF and composites.

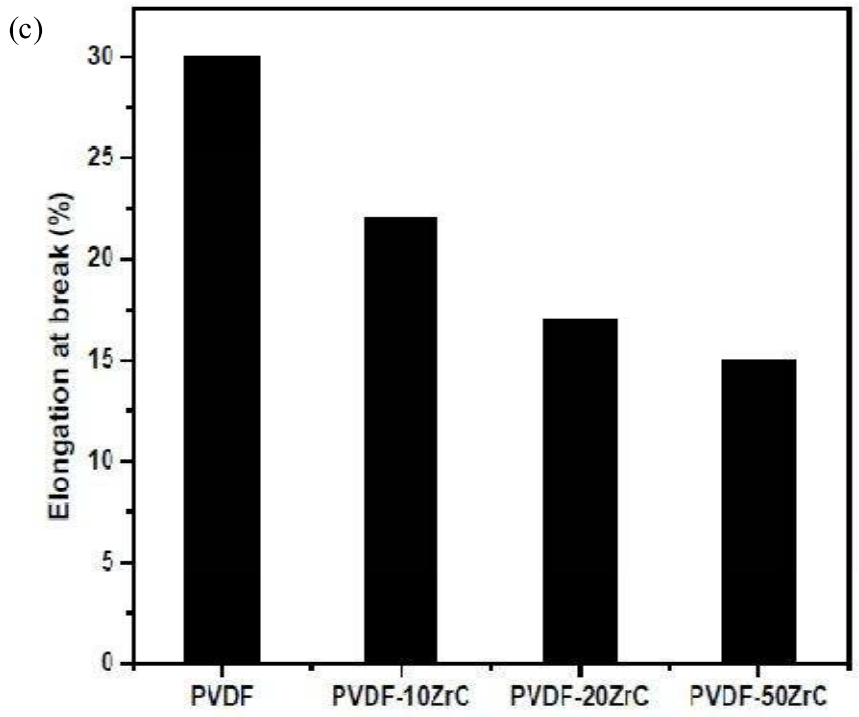

Figure 8.4 (c) Elongation at breaking point of PVDF and composites.

8.5. Dielectric properties

Dielectric permittivity of CCTO and CCTZO is 3100 and 21000 respectively at 100 Hz and 40^{o}C (Fig 8.5 a). CCTO has frequency independent ε' in the frequency range 1-10^6 Hz while frequency independent ε' in CCTZO is observed in the frequency range 10^2-10^6 Hz. Zr doping considerably increases the dielectric permittivity of CCTO. ε' of CCTO and CCTZO decreases rapidly with increase in frequency upto a particular frequency and thereafter it becomes almost independent of frequency. The frequency after which it becomes constant is more in CCTZO than that in CCTO. CCTO as well as CCTZO exhibits high value of ε' due to formation of barrier layers at the grains-grain boundaries interfaces [Sinclair et al (2002)]. In the case of composites, the dielectric permittivity increases with increasing content of CCTZO in PVDF (Fig. 8.5 e). Values of dielectric permittivity at 40^{0}C and 100 Hz for PVDF, PVDF-10ZrC PVDF-20ZrC and PVDF-50ZrC are 3.0, 32, 43 and 86 respectively. PVDF is present in α phase, which is

non-polar. Due to the non-polar nature of PVDF, the value of ε' is low. Dielectric permittivity increases with increasing temperature and decreasing frequency and vice versa (Figs 8.5 c, g, j and k). The composite materials always have microhetrogeneties due to the presence of two or more phases in electrical contact. There exists a difference in the conductivity of the dispersed phase/phases and the matrix. This gives rise to interfacial or space charge polarization due to blocking of the charge carriers at the polymer-ceramic interface. Space charge polarization involves displacement of charge carriers over large distance. Hence it cannot follow the alternating field at high frequency. This gives rise to rapid decrease in ε' with increase in frequency in the low frequency region. Variation of ε' with frequency at a few temperature for all the compositions are shown in figs 8.5 c, g, j and k. Figs 8.5 g, j and k shows similar behavior i.e. initially a rapid decrease in ε' with frequency in the low frequency region followed by a plateau above a certain frequency. Behavior of the composition PVDF-50ZrC is different from that of PVDF-10ZrC and PVDF-20ZrC. This composition exhibits a dielectric relaxation clearly in the frequency 10^1-10^2 Hz, the relaxing frequency shifts to higher frequency with increasing temperature. It is clear from the figure 8.5 (e), that ε' does not depend much on the frequency in the range 10^2-10^6 Hz. It is a desirable characteristic for electronic devices.

Tan δ vs log f plots for CCTO and CCTZO are shown in Fig 8.5 b. CCTO shows two peaks corresponding to two dielectric relaxation processes. The relaxation frequencies for both these dielectric relaxation are higher in CCTZO than CCTO. The higher frequency relaxation in CCTZO seems to occur beyond the frequency range of the instrument. Dielectric loss of CCTO does not change much with Zr doping. The value of tan δ for CCTO at 100 Hz and 40^0C is 0.86, which remains the same for CCTZO at the same frequency and temperature (Fig 8.5 b). The value of loss tangent for PVDF, PVDF-10ZrC PVDF-20ZrC and PVDF-50ZrC are 0.09, 0.09, 0.18 and 0.15 at 100 Hz and 40^0C respectively (Fig 8.5 f).

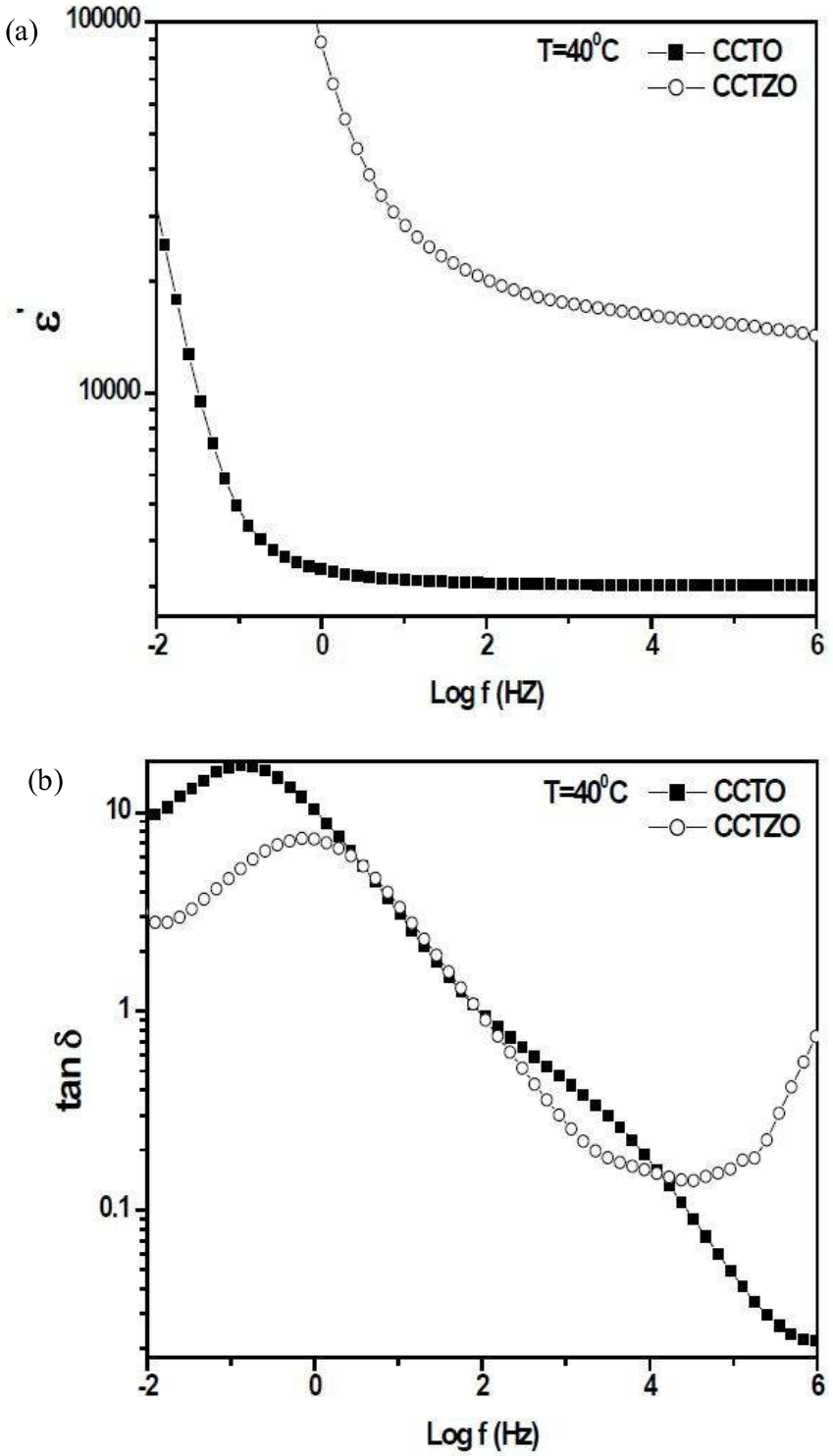

Figure 8.5 Frequency dependence of dielectric permittivity and tan δ (a and b) of CCTO and CCTZO at 40^0C

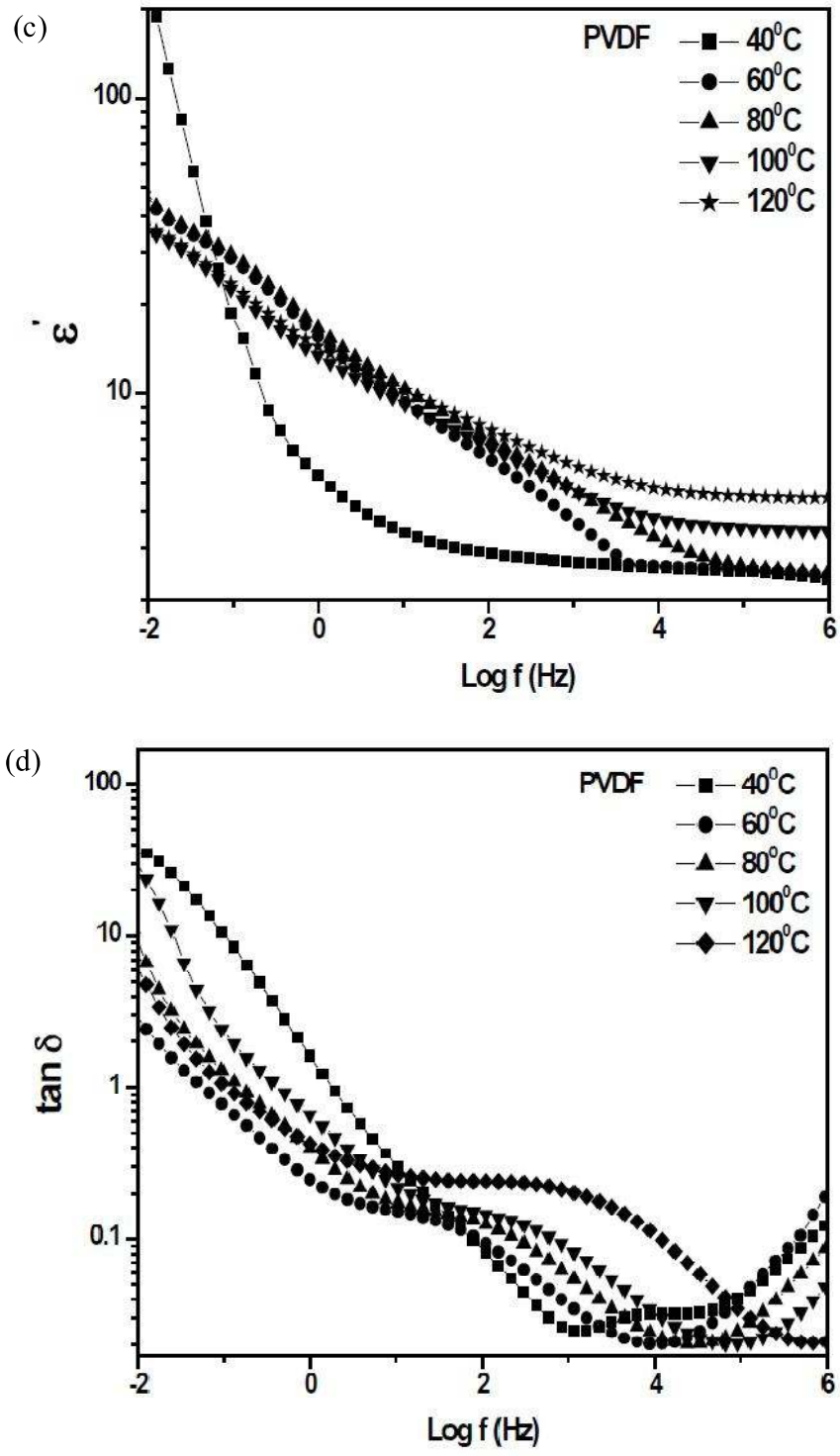

Figure 8.5 Frequency dependence of dielectric permittivity and tan δ (c and d) of PVDF at different temperatures.

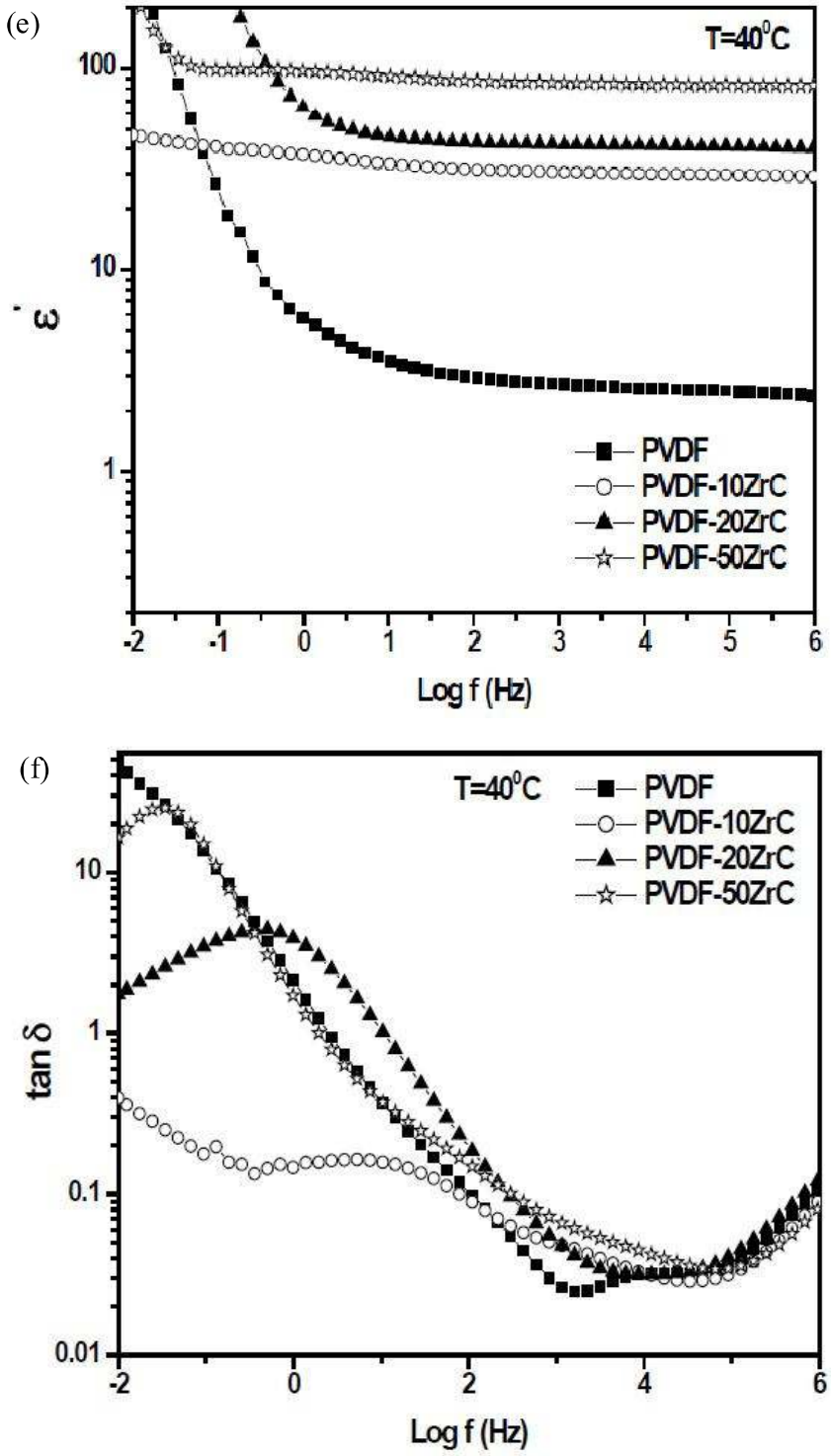

Figure 8.5 Frequency dependence of dielectric permittivity and tan δ (e and f) of PVDF and all the composites at 40^0 C.

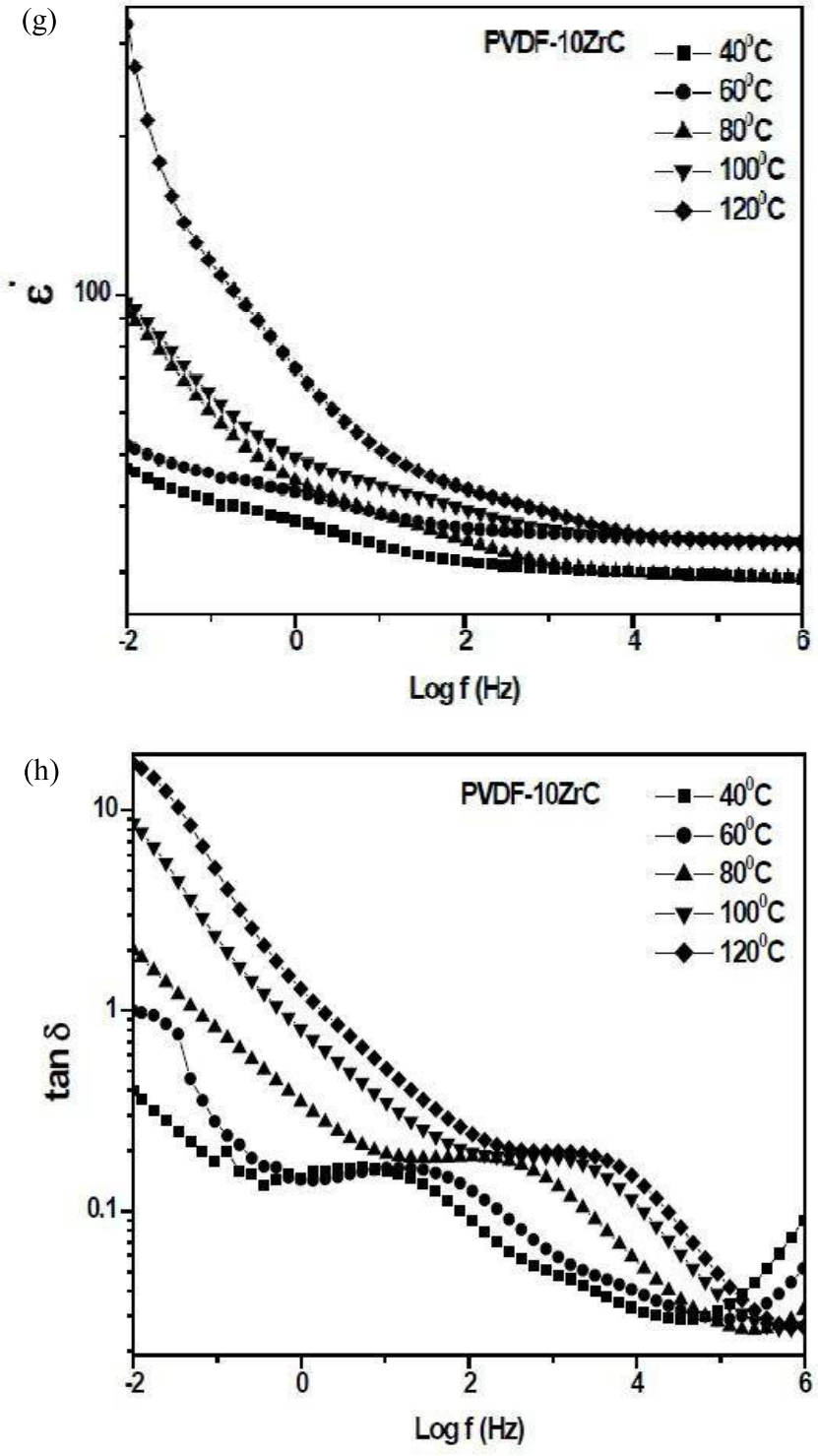

Figure 8.5 Frequency dependence of dielectric permittivity and tan δ (g and h) of PVDF-10ZrC at different temperatures.

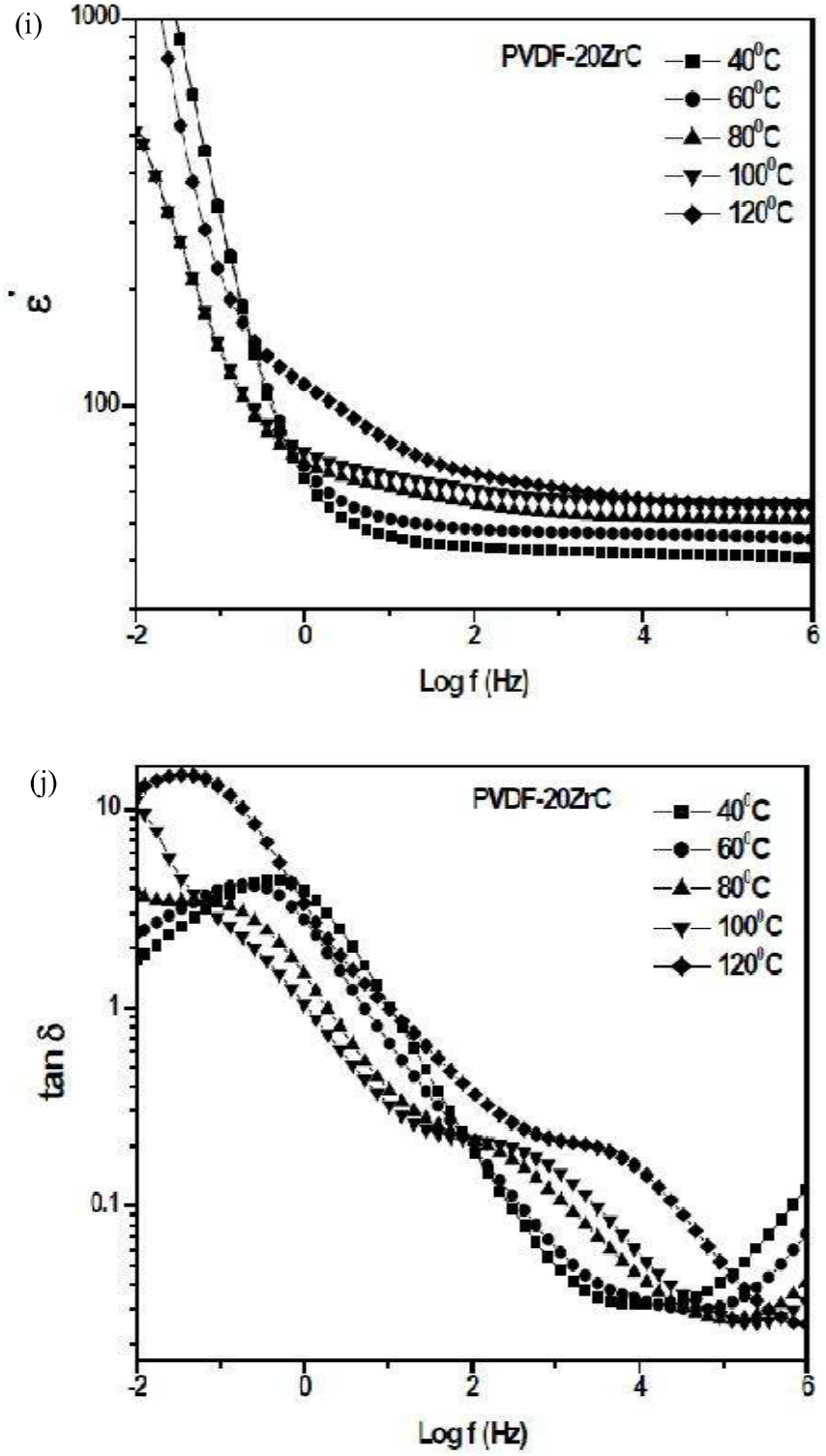

Figure 8.5 Frequency dependence of dielectric permittivity and tan δ (i and j) of PVDF-20ZrC at different temperatures

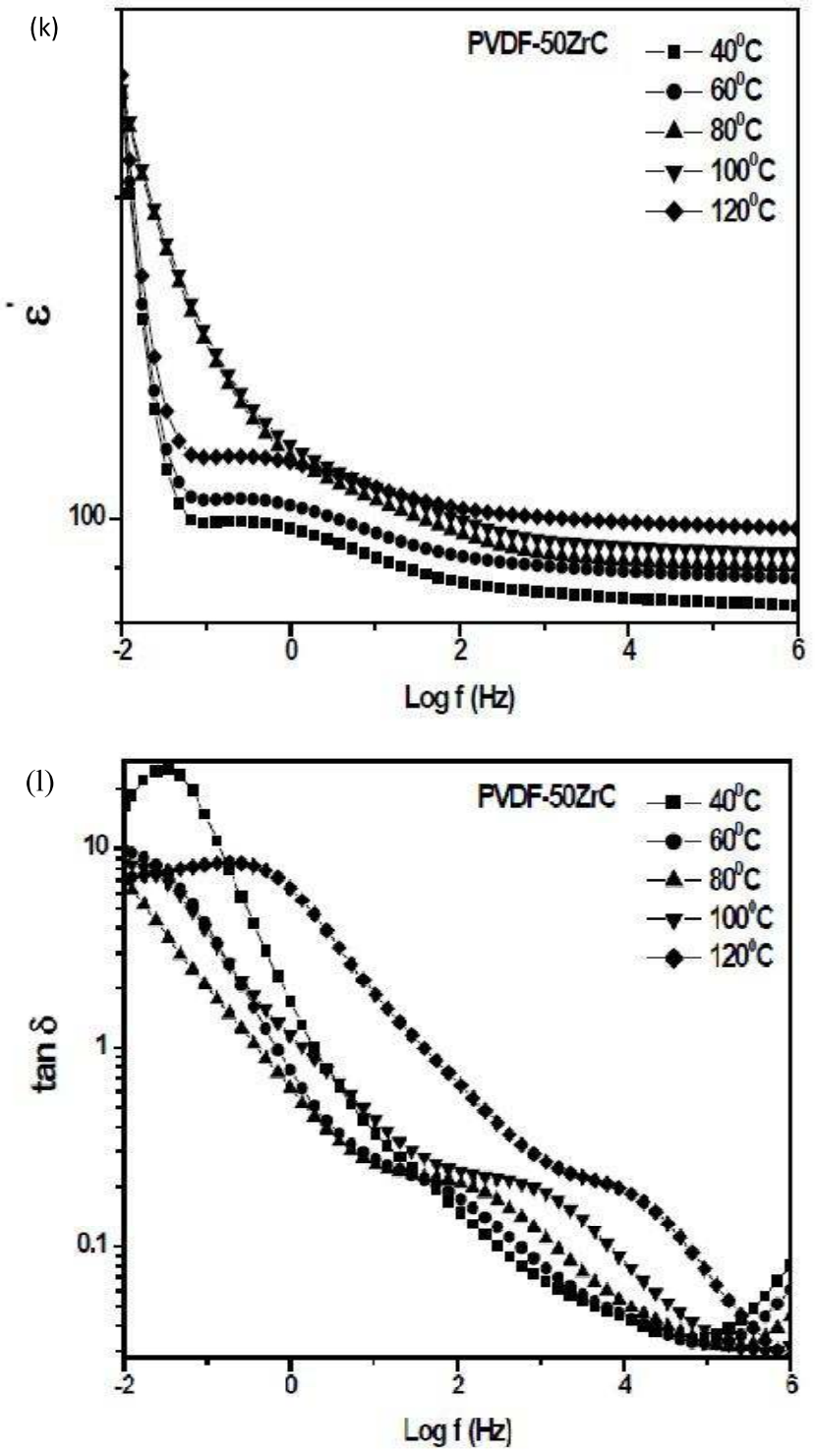

Figure 8.5 Frequency dependence of dielectric permittivity and tan δ (k and l) of PVDF-50ZrC at different temperatures.

A dielectric relaxation is observed at low frequency in the composites. Another dielectric relaxation is observed in the intermediate frequency range. These relaxations shift towards higher frequency with increasing temperatures (Figs 8.5 d, h, k and l). Low frequency relaxation is due to Maxwell Wagner polarization, while intermediate frequency relaxation is due to α_c relaxation associated with molecular motion of the polymer chains in the crystalline regions of PVDF. The glass transition relaxation α_a of PVDF occurs beyond 1 MHz (Fig 8.5 d) [Gregoria and Cestari (1994); Gregoria and Ueno (1999); Channel and Jog (2008)]. These relaxation peaks shift to higher frequency with increase in temperature, indicating lower relaxation time (τ). This seems to be due to the ease of relaxation because of decrease in the viscosity of the polymer with temperature.

To understand the nature of dielectric relaxation use is made of modulus spectroscopy. Electrical modulus is defined as inverse of the complex permittivity.

$$M^* = \frac{1}{\varepsilon^*} = \frac{1}{(\varepsilon' - J\varepsilon'')} = \frac{\varepsilon'}{(\varepsilon'^2 + \varepsilon''^2)} + \frac{J\varepsilon''}{(\varepsilon'^2 + \varepsilon''^2)} = M' + J.M'' \qquad (8.1)$$

where M', ε', and M", ε" are real and imaginary parts of the modulus and permittivity. The real M' and imaginary M" parts of electrical modulus are obtained as a function of frequency [Ramajo et al (2008); Hedvig (1977)]. It is observed from the figure 8.6 (a) that PVDF and the composites, there is a steep rise in the value of M' at a particular frequency. This frequency decreases with increasing content of CCTZO. This corresponds to a dielectric relaxation. A corresponding peak is observed in the M" vs log f plot at the same frequency.

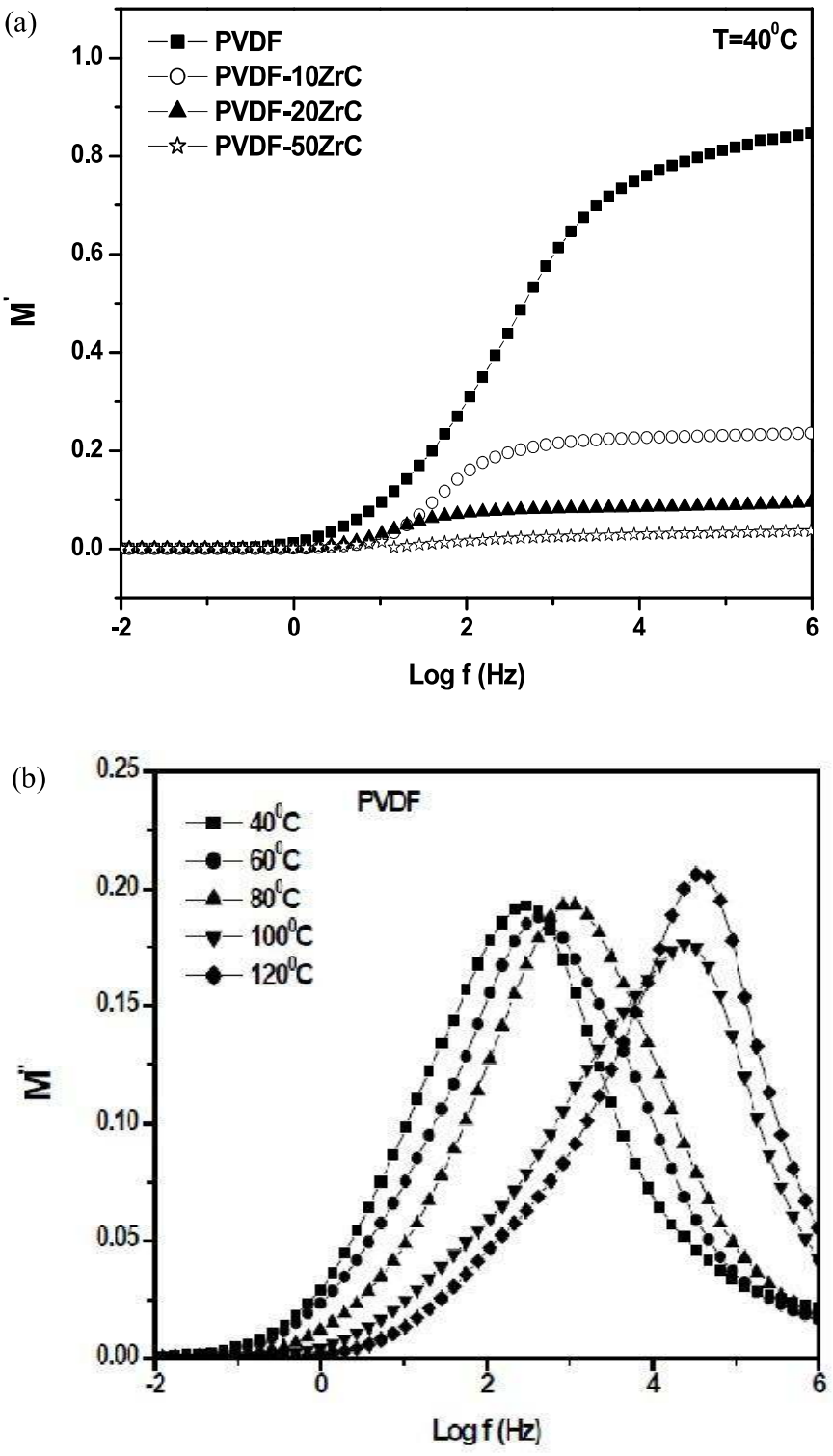

Figure 8.6 (a) M' vs log f plots of PVDF and composites at 40^0 C, (b) M'' vs log f plots of PVDF at different temperatures.

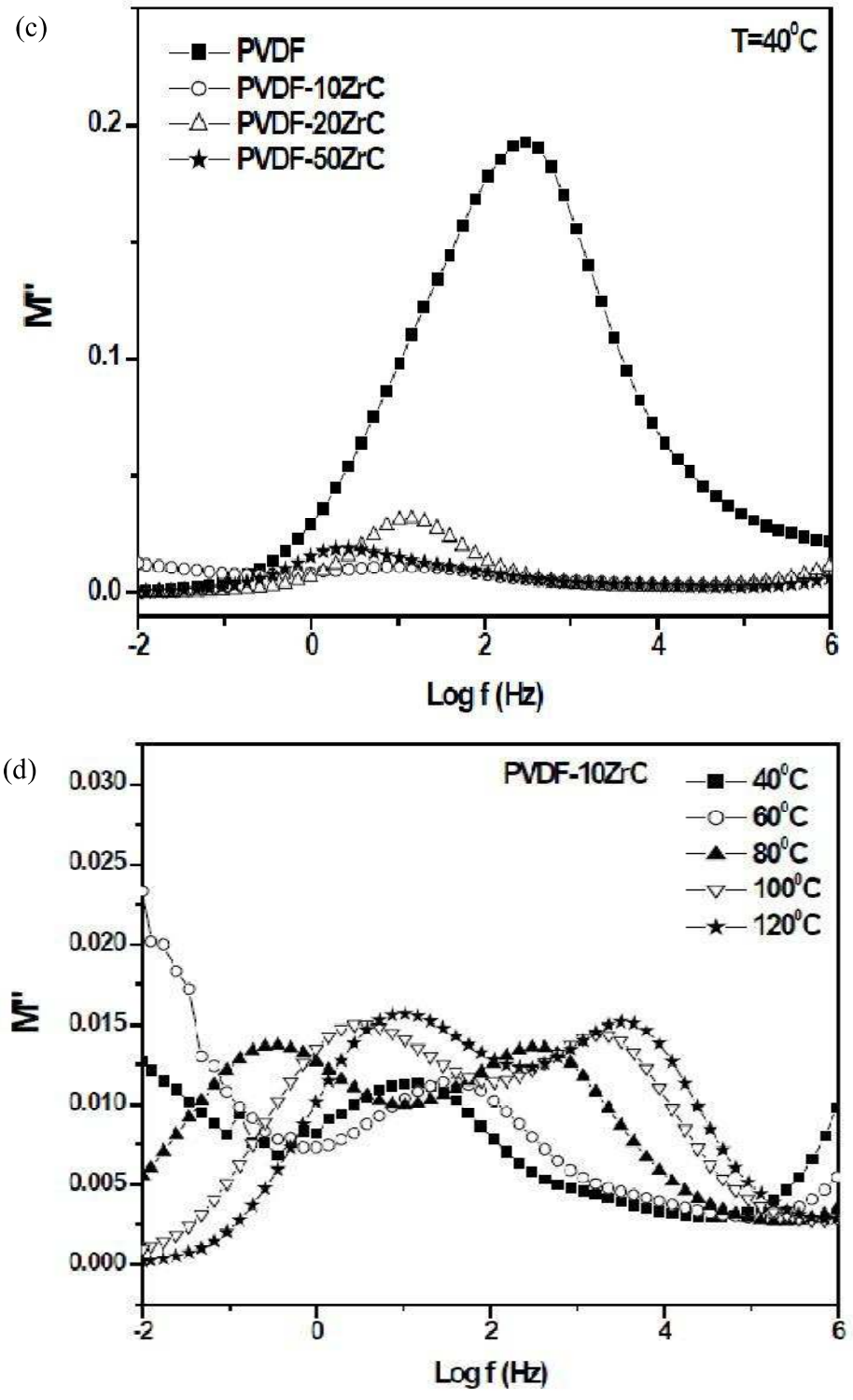

Figure 8.6 M'' vs log f plots of (c) PVDF and PVDF-ZrC composites at 40^0C, (d) PVDF-10ZrC at different temperatures,

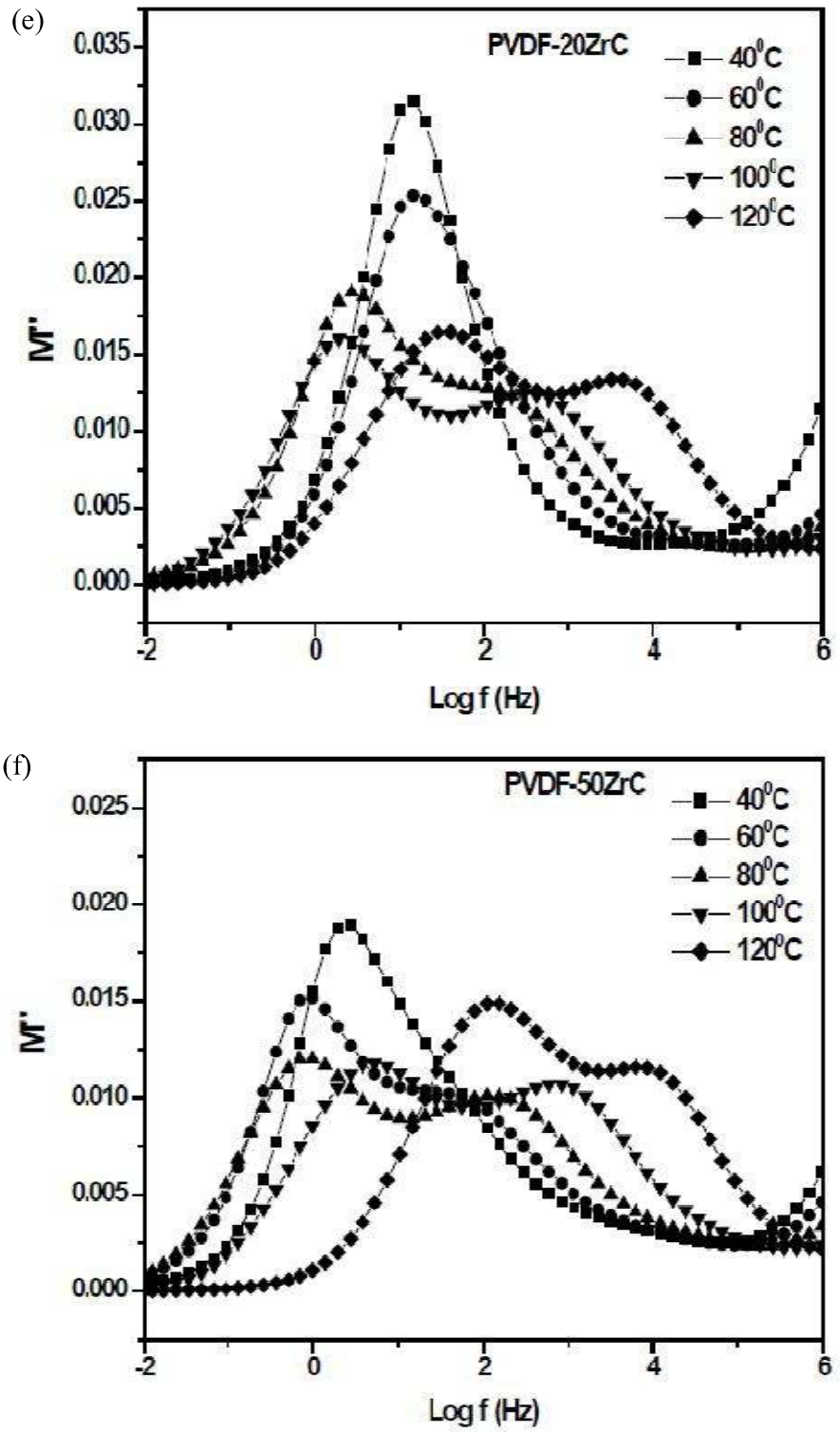

Figure 8.6 M" vs log f plots of (e) PVDF-20ZrC at different temperatures and (f) PVDF-50ZrC at different temperatures.

Fig 8.6 c shows M" vs log f plots of CCTZO, PVDF, PVDF-10ZrC, PVDF-20ZrC and PVDF-50ZrC at 40^0C. In the fig 8.6 b and c one relaxation appears in PVDF as well as composites. In PVDF this relaxation is observed around 100Hz (Fig 8.6 b). It is observed that with the increase in CCTZO content this relaxation peak shifts to lower frequency in composites. This is due to restricted mobility of polymeric chains because of their interaction with the filler particles. This relaxation is due to α_c relaxation associated with molecular motion of the polymer chains in the crystalline regions of PVDF. Height of the peak is less in the case of composites. This shows that the dielectric permittivity as well as the dielectric loss is more in the composites as compared to that in pure PVDF. These peaks shift to higher frequency with increasing temperature.

In the composites another peak appears at low frequency and high temperature (above 60^0C) (Fig 8.6 d-f). At 40^oC this peak is not observed in composites as it is present at much lower frequency. It is not observed in PVDF also. This relaxation is of Maxwell-Wagner-Sillar (MWS) type [Ramajo et al (2008); Hedvig (1977)]. Maxwell Wagner Sillar polarization is always present in multiphase systems having phases with different conductivities i.e. electrical heterogeneities. In such materials charge accumulates at the ceramic particles - polymer interface. This gives rise to space charge polarization leading to increase in the value of dielectric permittivity as well as the dielectric loss. As the dielectric permittivity of CCTZO is much higher than that of PVDF matrix, unbounded charges form large dipoles at the polymer matrix – ceramic interface. The induced dipoles find it difficult to follow the alternation of the electric field and thus the resulting relaxation process occurs in the low frequency region or at high temperatures.

Relaxation times, τ was determined using the relation $\tau = \frac{1}{2\pi f}$ where f is the frequency in cycles per second at the peak position in M" vs log f plots. Plots of log τ vs 1000/T for CCTZO, PVDF, PVDF-10ZrC, PVDF-20ZrC and PVDF-50ZrC is shown in fig 8.7. These plots are linear in accordance with Arrhenius relationship given below.

$$\tau_{max} = \tau_o \exp(\frac{E_R}{kT}) \quad (8.2)$$

where E_R is the activation energy associated with the relaxation process, τ_o the pre-exponential factor, k is the Boltzmann constant and T is the absolute temperature. Values of activation energy obtained from the slopes of these linear plots are given in Table 8.1. It is observed that the activation energy for α_c relaxation increases with increasing content of CCTZO. This may be due to increase in the stiffness with increasing content of CCTZO.

It is also noted that in M" vs log f plots of PVDF and composites (Fig 8.6 c) that with ceramic dispersion M" peaks shift to low frequency, with increasing content of CCTZO. This is because of the restriction in the movement of the polymer chains. Tensile test also confirms that with the increasing content of CCTZO, composites become stiffer.

Table 8.1. Activation energy from M'' vs log f plots.

Sample	Activation Energy
CCTZO	**0.51 eV**
PVDF	**0.70 eV**
PVDF-10ZrC	**0.76 eV**
PVDF-20ZrC	**0.77 eV**
PVDF-50ZrC	**0.96 eV**

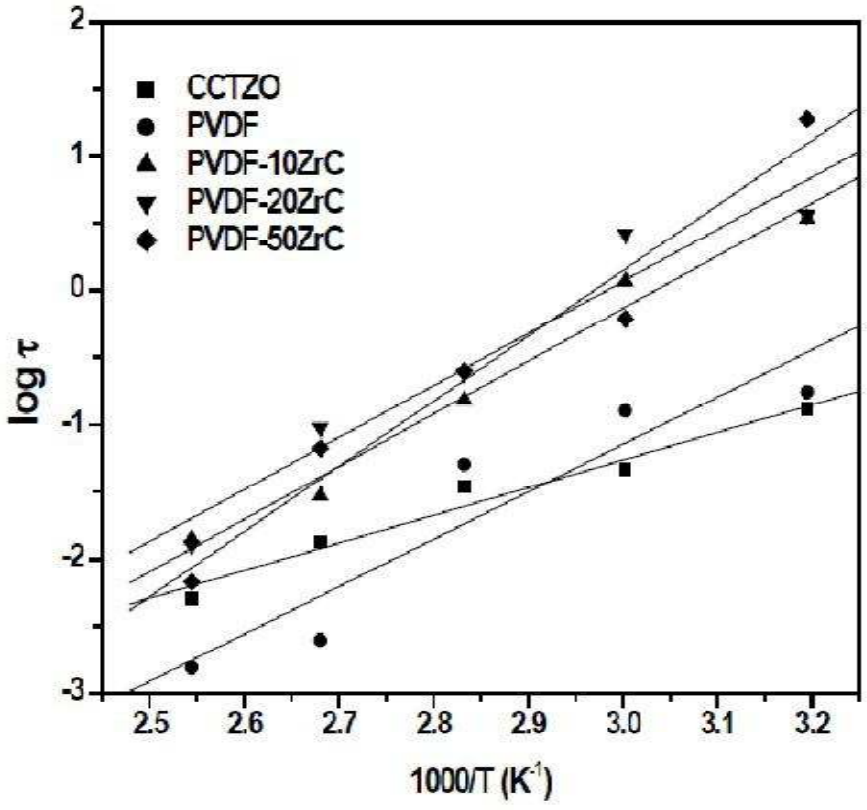

Figure 8.7 Log τ vs 1000/T curves for CCTZO, PVDF, PVDF-10ZrC, PVDF-20ZrC and PVDF-50ZrC.

Various models are used to predict the effective dielectric permittivity (ε' or ε_{eff} are the same) of the composites. The dielectric property of a biphasic dielectric mixture comprising of spherical crystallites with high dielectric permittivity and a matrix of low dielectric permittivity can be described by Maxwell's model [Maxwell 1954]. According to this model, the effective dielectric permittivity of the composite is given by

$$\varepsilon_{eff} = \frac{\delta_p \, \varepsilon_p \left(2/3 + \varepsilon_c/3\varepsilon_p\right) + \delta_c \, \varepsilon_c}{\delta_p \left(2/3 + \varepsilon_c/3\varepsilon_p\right) + \delta_c} \qquad (8.3)$$

where, ε_c, ε_p, δ_c and δ_p are the dielectric permittivity of CCTZO, PVDF, the volume fraction of the ceramic and the polymer respectively. After substituting the values of ε_c,

ε_p, δ_c and δ_p, the values of ε_{eff} obtained deviate much from the experimental values for all the wt fractions of CCTZO under study (Fig 8.8).

In the case of Clausius-Mossotti model [Frolich 1949], it is assumed that the mixture of dielectric is composed of spherical crystallites dispersed in a continuous medium. The effective dielectric permittivity (ε_{eff}) of the composite is given by the following equation.

$$\varepsilon_{eff} = \varepsilon_p \left[1 + 3\delta \left(\frac{(\varepsilon_c - \varepsilon_p)}{\varepsilon_c + 2\varepsilon_p}\right)\right] \qquad (8.4)$$

The predicted value of ε_{eff} using this model also deviates a lot from the experimental values (Fig 8.8). This may be due to non spherical shape of CCTZO particles as shown by SEM.

Lichtenecker's or logarithmic mixture rule is also used to predict the effective value of dielectric [Nalwa 1995]. According to this model ε_{eff} is given by

$$\text{Log}\, \varepsilon_{eff} = \delta_1 log\varepsilon_1 + \delta_2 log\varepsilon_2 \qquad (8.5)$$

Experimental results are significantly different from the predicted results using this model also (Fig 8.8). This is because Logarithmic law is applicable only when there is not much difference in the value of ε' of the dispersion medium and the dispersed phase. This is not true in the case of PVDF-ZrC composites. ε' of CCTZO is far greater than ε' of PVDF. Therefore the experimental results do not match exactly with values predicted by this model.

The effective medium theory (EMT) model [Rao et al (2000)] has been developed taking into account the morphology of the particles. According to this model, ε_{eff} is given by

$$\varepsilon_{eff} = \varepsilon_p[1 + \frac{f_c(\varepsilon_c - \varepsilon_p)}{\varepsilon_p + n(1-f_c)(\varepsilon_c - \varepsilon_p)}] \qquad (8.6)$$

Where f_c is the volume fraction of the ceramic dispersed, ε_c, ε_p and *n* are the dielectric permittivity of the ceramic, polymer and the ceramic morphology fitting factor respectively. The experimental values obtained are closest to the predicted values in this case of all the models employed to predict the ε_{eff} values. The shape parameter n has been found to be 0.061.

All these models have the limitations that the chemistry of interfacial structure has not been taken into account and particles are assumed to be of spherical shape. Microstructure and microchemistry of the interfaces are also very important to determine the physical, mechanical and electrical properties of the composites. Therefore the experimental results do not match exactly with values predicted by these models.

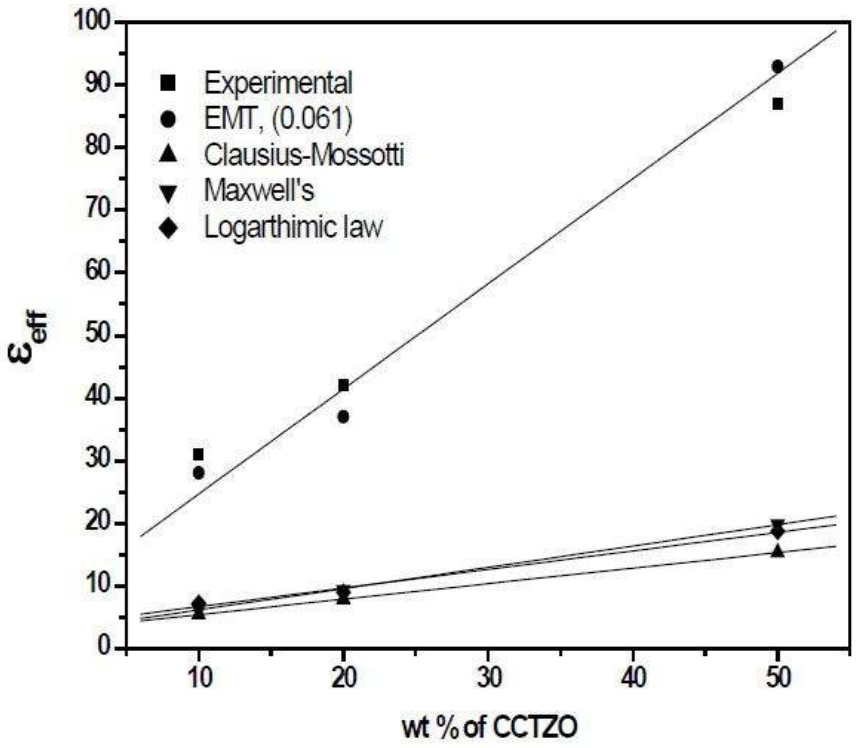

Figure 8.8 Variation of effective dielectric permittivity (ε_{eff}) measured at 100 Hz and 40^{o}C for PVDF-ZrC composites based on various models.

Temperature-dependence of dielectric relaxation is explained by Havriliak-Negami (H-N) function [Windlass et al (2001); Mijovic et al (2006)]:

$$\varepsilon^{*} = -i\frac{\sigma_{dc}}{\varepsilon_0 \omega^{s}} + \varepsilon_{\infty} + \sum_{j}\frac{(\Delta\varepsilon)_j}{[1+(iw\tau_j)^{\alpha}]^{\beta}} \qquad (8.7)$$

where, σ_{dc} is dc conductivity, ω is the angular frequency, s is an exponent ($0<s \leq 1$), τ_j is the relaxation time of the j^{th} process, ε_0 is the vacuum permittivity, $\Delta\varepsilon$ is the dielectric strength of the j^{th} process and α and β are the shape parameters of the H-N function which define the symmetric and asymmetric broadening of the α_c relaxation peak in ε'' curve. Analysis of H-N function using WinFit software program of PVDF and PVDF-50ZrC composite have been given in Table 8.2 using deconvoluted H-N fits presented in (Fig.8.9). The exponent parameter, α represents the slope of the lower frequency side of the relaxation peak in ε'' curve. β is the asymmetry parameter which is calculated from the slope of higher frequency side of the same curve as α. The higher value of α for composites as compared to pure PVDF indicates a stretched relaxation over a wider range of frequencies. Where $0<\beta\leq1$ leads to asymmetrical broadening for the relaxation function. For $\beta=1$ the Debye-function is obtained. Asymmetry parameter β has a value of 1 for PVDF showing the symmetry of the spectrum. For the composites, β parameter has different values due to the dispersion of ceramics particles which creates heterogeneity in the system. For composites, the relaxation time (s) calculated from H-N fit decreases with increase in temperature. The composites exhibit lower relaxation time as compared to PVDF. Exact reason for this is not clear at present. With increase in the temperature, the relaxation time decreases in the composites. Lower value of relaxation time at higher temperature is because of the ease of relaxation at higher temperature due to increased mobility of the chains both for pure PVDF as well as composites.

Table 8.2 Fitting parameters for α_c relaxation as a function of temperature obtained from H-N fits.

Temp	PVDF, α	PVDF-50ZrC, α	PVDF, β	PVDF-50ZrC, β	PVDF, τ	PVDF-50ZrC, τ
40	0.49	0.62	1	0.58	2.33E-2	5.45E-2
80	0.53	0.64	1	0.62	1.45E-3	6.26E-4
120	0.57	0.71	1	0.69	7.44E-4	3.67E-5

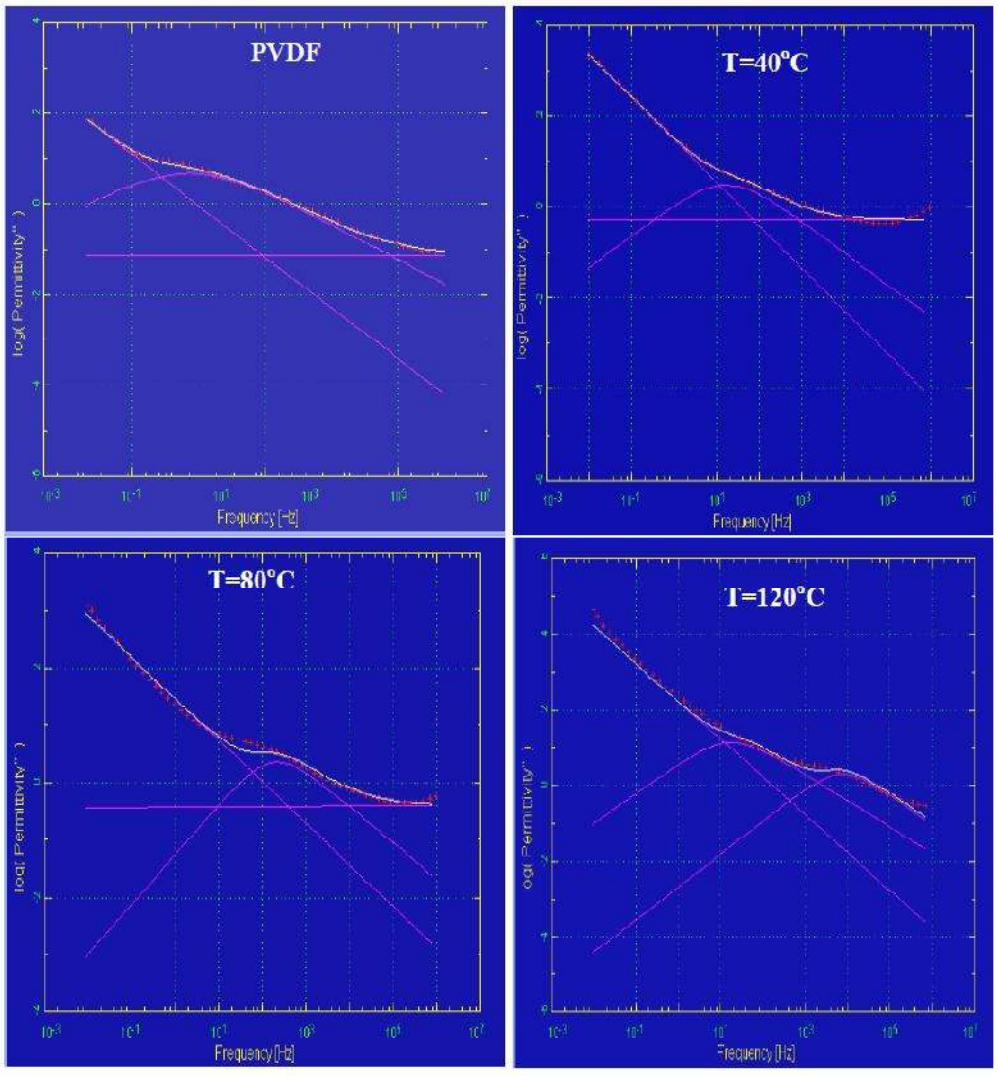

Figure 8.9 Dielectric loss in the frequency domain and spectrum was deconvoluted from H-N fits for PVDF-50ZrC.

8.6. Conclusion

- $CaCu_3Ti_4O_{12}$ and Zr doped $CaCu_3Ti_4O_{12}$ (CCTZO) have been prepared by solid state conventional technique.

- CCTZO dispersed PVDF composites have been prepared by melt extrusion process.

- There is no structural change as indicated by powder XRD studies.

- Zr doping substantially increases the dielectric permittivity and decreases the dielectric loss in CCTO. Dielectric permittivity increases with increase in the content of CCTZO in the composites.

- Dielectric loss in the composites is slightly higher than the pure PVDF but less than that of CCTZO.

- As the filler content increases in the PVDF matrix, M' decreases. In the modulus spectroscopy two dielectric relaxations have been observed in the composites. One relaxation occurring at low frequency is of Maxwell-Wagner-Sillar (MWS) type, while the other relaxation occurring in the intermediate frequency range is due to α_c relaxation associated with molecular motion of the polymer chains in the crystalline regions of PVDF.

- Temperature dependence of dielectric relaxation has been studied in details using H-N function. Debye type relaxation is observed in pure PVDF with $\beta=1$. Stretched relaxation over a wider range of frequencies has been observed in the composite suggesting asymmetric nature of relaxation.